Journal of Molecular Liquids 367 (2022) 120467

Contents lists available at ScienceDirect

Journal of Molecular Liquids

journal homepage: www.elsevier.com/locate/molliq

Stable hazy states by electrohydrodynamic convection of ultraviolet-treated chiral nematic liquid crystal

Jeong Won Ryu [a], Gyu-Jin Choi [a], Chao Ping Chen [b], Chul Gyu Jhun [c,*], Jin Seog Gwag [a,*]

[a] Department of Physics, Yeungnam University, 280 Daehak-Ro, Gyeongsan, Gyeongbuk 38541, Republic of Korea
[b] Smart Display Lab, Department of Electronic Engineering, Shanghai Jiao Tong University, Shanghai 200240, China
[c] Department of Digital Display Engineering, Hoseo University, Asan-si, Chungcheongnam-do 31499, Republic of Korea

ARTICLE INFO

Article history:
Received 29 June 2022
Revised 29 August 2022
Accepted 22 September 2022
Available online 27 September 2022

Keywords:
Electrohydrodynamic convection
Chiral nematic liquid crystal
Stable state
Haze
Smart window
UV-irradiation

ABSTRACT

In this paper, we show that electrohydrodynamic convection of ultraviolet (UV)-treated chiral nematic liquid crystals (CNLCs) generates stable foggy states. UV-irradiation produces relatively heavier and larger molecular ions at CNLC mixture, which activates electroconvection, and leads to easily dynamic scattering mode (DSM) with strong turbulence. Chirality of LC combined with the DSM builds two stable states (planar state and focal conic state) more strongly, unlike the conventional method generating the two states in the CNLCs. The molecular ion effect enables state conversion to a much lower switching voltage than that of the conventional cholesteric devices. The focal conic state connected to DSM2 exhibits a stable deep hazy state, the mixed state combined with DSM1 displays a stable weak hazy state, and the planar state activated in a particular frequency region creates a stable and very clear transparent state due to the chiral pitch of the infrared region. Therefore, a smart window with the tri-stable-hazy state specialized in low power consumption can be realized. The tri-stable-hazy state device also generates various hazy states according to the applied voltage; thus, it can provide a proper indoor temperature for users. Furthermore, a stable planar state with a chiral pitch designed in the infrared region may save energy through selective reflection of infrared rays from the sunlight in the summer. The proposed technology is suitable for commercial use in the next-generation smart window.

© 2022 Elsevier B.V. All rights reserved.

1. Introduction

Smart windows have attracted considerable attention in the construction, automobile, and interior design industries because they enable personal privacy protection, pleasant indoor environments, and reduced energy consumption. Various smart windows that scatter, reflect, or absorb visible and infrared light have been developed for these purposes [1–19]. A representative technology applied to light-reflection-type smart windows is a typical cholesteric liquid crystal that shows a Bragg reflection effect that reflects any specific wavelength depending on the chiral pitch of liquid crystals (LCs) [8–12]. However, this requires the use of a higher driving voltage that poses the risk of electric shock in the transition between two stable states (planar state and focal conic state). In addition, the two states are not stable enough for use in smart windows. The conventional technologies applied to light scattering-type smart windows are polymer dispersed LC that change haze by electrically controlling the difference between the refractive index of the polymer and the extraordinary refractive index of the LC [13–19]. However, this approach has disadvantages such as the use of a high driving voltage that poses the risk of electric shock and the narrow viewing angle in the transparent state so that scattering occurs at the side view because the refractive indices of the LC and the polymer at the side view are optically mismatched. Therefore, it is urgently necessary to develop a smart window with excellent viewing angle, low manufacturing cost, low power, and low driving voltage.

Generally, nematic LC with opposite signs of electrical conductivity anisotropy and dielectric anisotropy generate electrohydrodynamic convection (EHC) under an electric field and exhibit a characteristic variety of patterns in fluid systems [20–30]. The shape of the pattern changes with the amplitude, frequency, and waveform of the electric field. The representative EHC pattern is the Williams domain that arises due to the Carr–Helfrich instability and emerges in the low-frequency and low-electric-field conduction regime [31]. At a low electric field, the period of patterns and the size of the LC domain are larger than the wavelength of light; therefore, even if the LCs exhibit birefringence, they rarely

* Corresponding authors.
E-mail addresses: cgjhun@hoseo.edu (C. Gyu Jhun), sweat3000@ynu.ac.kr (J. Seog Gwag).

https://doi.org/10.1016/j.molliq.2022.120467
0167-7322/© 2022 Elsevier B.V. All rights reserved.

scatter and appear transparent. However, as the applied electric field becomes stronger, the regular arrangement of the LCs collapses, the periodic radius of the curvature becomes very small, and a dynamic scattering mode (DSM) begins to appear in which the direction of motion changes from a specific to a random direction. DSM is not only directionless but also very fast and has a very small LC domain; thus, light scattering occurs with a strong turbulence phenomenon. In the DSM1 region, where the electric field is relatively weak, relatively large and low-density disclination defects begin to be generated that act as the nuclei of scattering and become the domain of liquid crystal scattering. This causes weak scattering. As the electric field becomes stronger, the density of the disclination defects increases rapidly and the domain size becomes very small, generating a rapidly growing DSM2 region where strong light scattering occurs. Therefore, attempts have been made to use DSM2 as a haze state for smart windows. To lower the driving voltage, ionic additives that activate electroconvection, such as tetra-*n*-butyl-ammonium bromide (TBAB), should be doped into LCs. However, ionic additives not only accumulate charge in the electrode, but also generate a voltage drop phenomenon and reduce the life of the device by generating electrical current. Roman Dabrowski et al. showed excellent dynamic scattering and memory properties in new fluorinated smectics synthesized for the application of smart windows and memory displays. However, the smectic LCs still has the issue of alignment stability, leaving questions about its actual application and it also cannot be free from electrical degradation because it also uses ionic additives [32].

Thus, for applying LC electroconvection technology to smart window, it is necessary to develop a technology to lower the driving voltage without electrical degradation of LC cell.

In this paper, we present a smart window technology with low power consumption and low driving voltage based on LC electroconvection. To reduce the driving voltage, LCs were irradiated with strong ultraviolet light (UV) to dramatically activate LC electroconvection without any ion additives. The UV-irradiated LC mixture behaved as heavy molecular ions in the electric field, producing DSM2 at low voltages without dielectric breakdown. A low-power smart window with a tri-stable state was achieved using chiral LCs. The molecular ion effect generating at LC mixture by UV irradiation enables state conversion to a much lower switching voltage than that of the conventional cholesteric devices. The chiral pitch in the infrared region shows the effect of energy saving through the selective reflection of infrared rays. Consequently, a smart window with a high switching speed, excellent viewing angle characteristics, low manufacturing cost, low power, and low driving voltage is realized using improved LC EHC technology.

2. Materials and methods

2.1. Materials

SLC10V512-300 was used as an LCs for all experiments and purchased from Slichem Co. ltd. The birefringence, dielectric anisotropy, and nematic-isotropic transition temperature of SLC10V512-300 are 0.2, −13.2, and 90 °C, respectively. The homeotropic LC alignment layer, DL-4027, was purchased from H. K. Microscience International, ltd. TBAB was purchased from Sigma–Aldrich. S811 was purchased from PharChem, Inc. All chemicals were used directly without further purification.

2.2. Device fabrication

Glass substrates were cleaned ultrasonically with ethanol and deionized water and dried on a hot plate at 120 °C for 10 min. Indium-tin oxide (ITO) coated on the bottom glass substrate with a size of 3 cm × 4 cm was used as the electrode. The ITO-coated glass substrates were spin-coated with polyimide DL-4027 to obtain homeotropic LC alignment followed by prebaking at 110 °C for 5 min and curing at 220 °C for 1 h. The gap between the LC cells was approximately 10 μ μm. SLC10V512-300 was used as the LC. To generate chiral LC states in the cells, S811 that leads to the left-handed chirality of the LC was selected as the chiral dopant. The LCs with chiral dopants were injected into the sandwich LC cell and then sealed with a photocurable polymer.

2.3. Material and device characterizations

A NIPPON Denshoku Haze Meter-400 instrument was used to measure the haze of the LC cells, and the LC textures were observed using an Olympus-Scope BX41 microscope. NMR spectra were recorded using an Agilent Technologies V NMR NMR spectrometer (600 MHz). The voltage applied to the LC cell was provided by a waveform generator (AFG3022B, Tektronix). A voltage amplifier provided by FLC Electronics, A400D was used to amplify the voltage. The resistances of the LC cells were measured using a Keithley 2400 SourceMeter. KJPHT-101 (KJUV) was used as the UV-exposure equipment. The intensity of the UV irradiation on the LC cell was measured using a Model 1918-C Newport Power Meter.

3. Results and discussion

The EHC instability effect in LCs is caused by the reorientation of nematic LCs with the motion of charged molecules in an electric field. In the absence of charged molecules in the form of ions in the LC cell, the EHC phenomenon does not occur under an alternating current (AC) field. Thus, to activate EHC, a small amount of ionic molecules is added to the LCs, increasing the conductivity and reducing the driving voltage of the LC system. However, mobile charged molecules tend to accumulate on the electrodes under an electric field, which may result in a voltage drop inside the LC cell due to the additional electric potentials generated by the accumulated charged ions. Ultimately, such charge accumulation can also dramatically increase the electrical current in the LC device, even at a voltage that is not very high, resulting in damage caused by dielectric breakdown.

To activate EHC without using ionic additives, we considered a method of making minute changes to the chemical structure of the LCs. The most suitable methods for this purpose are low-energy ion-beam treatment, low-energy electron-beam treatment, and ultraviolet irradiation. However, because LCs cannot be used in vacuum processes, ion- and electron-beam treatments were excluded, and UV irradiation at a wavelength of 365 nm was selected.

Figure S1 shows frequency region generating DSM2 for UV treated LC sample and LC sample with TBAB. For the ionic molecules produced at LC mixture by UV irradiation, the frequency that generates turbulent LC flow or DSM2 at the lowest voltage is less than 200 Hz unlike general ion additives like TBAB which produces the DSM2 at with relatively high frequency (∼5 kHz). It would mean that the ionic molecule generating at LC mixture by UV irradiation is relatively heavier and larger molecule and thus, moves slowly under electric field. Its mass is considered to be at least five times greater than that of the bromine ion in TBAB by applying the Stokes Law on the movement of particles in fluid under the electric field, when comparing the frequencies. Fig. 1 shows a schematic diagram of behavior of UV irradiated LC mixture. At low frequencies, when the polarity of the voltage changes, sufficiently large motion of the heavy ion (molecular ion) is generated, creating a turbulent convection flow of LCs which appears as dynamic light scattering;

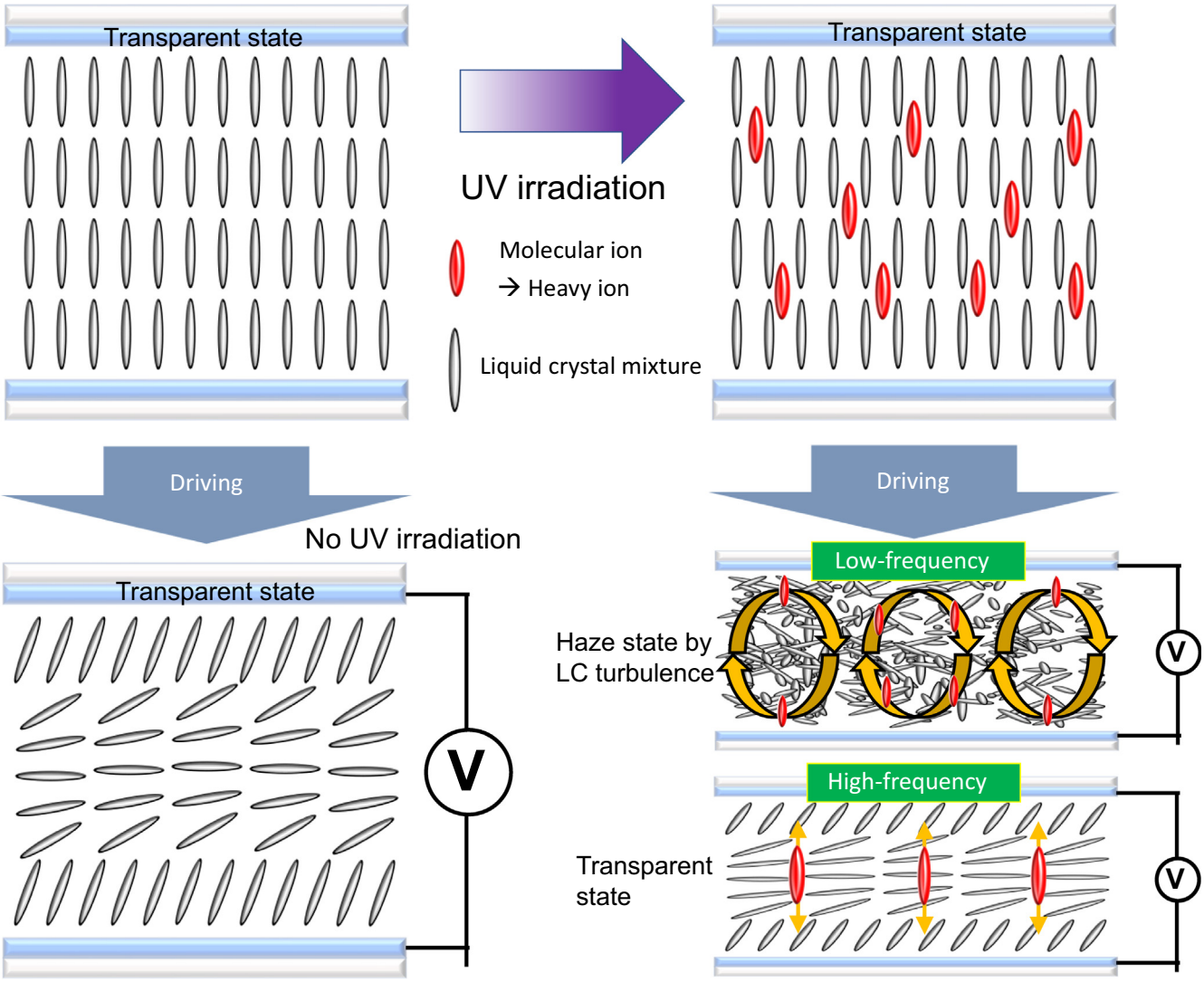

Fig. 1. Simple schematic diagram of the behavior of UV irradiated LC mixture.

however, at high frequencies, the polarity of the voltage changes before the molecular ion can move so that the electroconvection of the LCs cannot be driven. Therefore, the turbulent flow of the LCs at higher frequencies may be created under stronger electric field which exerts a great Coulomb force on the heavy ions.

SLC10V512-300 provided by Slichem Co., ltd. was used as the LC with negative dielectric anisotropy and was treated by UV irradiation at various intensities and exposure times. The UV-irradiated LCs were injected into a sandwich cell made of two glass substrates coated with a homeotropic alignment layer (DL-4027 provided by H. K. Microscience International, ltd.) on an indium tin oxide (ITO) electrode thin film. Generally, the switching voltage to DSM2 is considerably reduced in the LC cell using UV-irradiated LCs combined with the homeotropic alignment layer compared to the LC cell with UV-irradiated LCs coupled to the planar alignment layer. This is because LCs with negative dielectric anisotropy that are horizontally aligned do not move under the vertical electric field, whereas the homeotropically aligned LCs move rapidly toward the planar orientation under a vertical electric field. Consequently, the movement of LCs can further activate the EHC. To confirm the difference between the UV-irradiated LC cell and the LC cell containing the ionic additive, each LC cell was fabricated, and the difference in the switching voltage was compared to that of DSM2 (Fig. 2(a–c)). An untreated LC cell did not produce a general convection pattern such as the Williams domain or grid pattern even at the very high voltages of 80 V or higher in all frequency regions (Fig. 2(a)). By contrast, LC cells containing ionic additives and UV-irradiated LC cells showed typical EHC patterns, and the switching voltages to DSM2 were relatively low at 30 V (Fig. 2(b)). TBAB was used as an ionic additive and its content in the LCs was 0.1 w% (Fig. 2(b)). The UV-irradiated LC (The UV intensity and irradiation time were 150 mW/cm^2 and 4 min, respectively) showed an effect on the EHC instability similar to that of the LC with ionic additives; that is, it can be inferred that a charged material was generated in the LCs by UV irradiation (Fig. 2(c)). Therefore, dielectric breakdown will occur in the UV-irradiated LC cell under an appropriately high voltage, as shown in Figure S2. However, even at high voltages, no dielectric breakdown was observed in the UV-irradiated LC cells, similar to the untreated LC cells (Figure S3). We explain this interesting phenomenon as follows. The UV irradiation is generating the exited states and can form radicals, which can initialize the radical or ionic-radical reaction and post processes. Depending on the irradiation dose and wavelength, the level of degradation can affect lower or bigger fraction of mixture. From our experimental results, we have mentioned that the ionic molecules produced by ultraviolet irradiation are large and heavy. Thus, we assume that

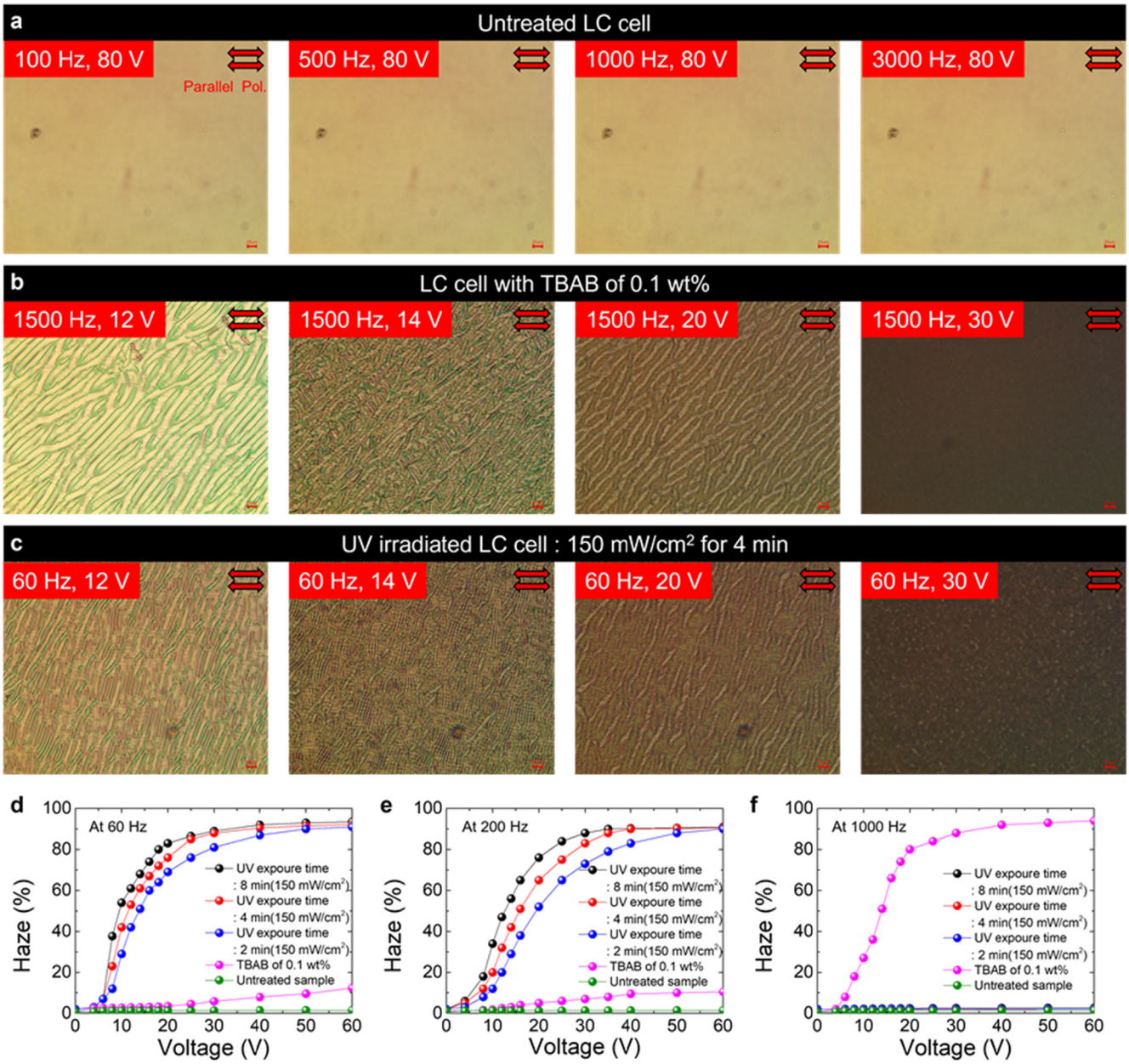

Fig. 2. Microscopic images of convection patterns (**a**) Microscopic images according to frequency and voltage in untreated LC cell (**b**) Microscopic images according to frequency and voltage in LC cell with TBAB OF 0.1 w%. (**c**) Microscopic images according to frequency and voltage UV irradiated LC cell. (**d**) Haze depending on voltage of 60 Hz for untreated LC cell, LC cell with TBAB OF 0.1 w%, and UV irradiated LC cell. (**e**) Haze depending on voltage of 200 Hz for untreated LC cell, LC cell with TBAB OF 0.1 w%, and UV irradiated LC cell. (**f**) Haze depending on voltage of 1000 Hz for untreated LC cell, LC cell with TBAB OF 0.1 w%, and UV irradiated LC cell.

some of the LC mixture have been ionized by UV irradiation. Because these ionic LC molecules are large, their charge density and moving speed are much lower than atomic ions such as bromine, so the current density flowing in the LC fluid will be much lower. Even if they accumulate on the surface of the LC alignment layer, it will be difficult to penetrate the alignment layer. This is presumed to be the reason why UV irradiated LS cells do not cause dielectric breakdown even at high voltages. In addition, in the conventional method, LC convection is induced by ionic additives, but for UV irradiation method, LC mixture itself acts as a source of LC convection so that the dynamic light scattering effect may be great.

Fig. 2(d–f) show haze as a function of voltage at 60, 200, and 1000 Hz, respectively, for the untreated LC sample, LC sample with TBAB of 0.1 w%, and LC samples irradiated by UV for 2, 4, and 8 min at 150 mW. As expected, it can be seen that at a relatively low frequency of 60 Hz, the haze of the untreated LC cell and the LC cell with the TBAB hardly increases even at a high voltage. In contrast, for the UV-irradiated LC samples, the sample with long UV irradiation time showed relatively high haze for the same voltage, and the maximum haze was 91 % (Fig. 2(d)). The dependence of haze on the voltage at 200 Hz was almost the same as that shown in Fig. 2(d) even though the voltage of the UV-irradiated sample necessary to obtain the same haze increased slightly (Fig. 2(e)). As predicted, the dependence of haze on the voltage at a relatively high frequency of 1000 Hz was the opposite of that shown in Fig. 2(f). The UV-irradiated LC samples rarely reacted to the voltage at this frequency, but the TBAB LC cell containing light ions showed a clear change in the haze with the voltage (Fig. 2(f)). Consequently, the different electroconvection mechanisms of the UV-irradiated LC cells and TBAB LC cells can be confirmed through the different

frequency-dependent regions of the two LC cells. The results for LC cells under more diverse UV irradiation conditions are shown in Figure S4. It is observed from Figure S4 that the optimal UV irradiation time is 8 min. In all subsequent experiments, UV irradiation was performed for 8 min at 150 mW.

To confirm the effect of the UV-irradiated chiral nematic LCs (CNLCs) on EHC, we investigated the voltage and frequency dependence and holding time of the states by irradiating CNLC cells with various chiral dopants. Fig. 3(a–c) show the changes in the haze with the variations in the voltage, amount of chiral dopant, and frequency of the UV-irradiated CNLC samples, respectively. Fig. 3(a) shows the haze change with the variation of the voltage at a frequency of 60 Hz when the amount of chiral dopant was changed from 0 to 9 wt%. With increasing concentration of the chiral dopant, a high voltage was required to obtain the same haze, except for the chiral concentration of 0 wt%. This may be because for weak chirality, the force to activate the EHC is greater than the elasticity by twist, which is effective in LC EHC. However, strong chirality increases the elasticity by twist, adversely affecting the LC EHC. Fig. 3(b) shows the haze change with the amount of the chiral dopant at a voltage of 20 V when the frequency was changed from 30 to 1000 Hz. It is observed that these results once again show the frequency dependence of the UV-irradiated LC samples on haze. With exception of the results for 0 wt%, lower frequency and chiral concentration correspond to higher haze. Fig. 3(c) shows the haze change depending on the frequency at the chiral dopant content of 3 wt% for the voltages of 10, 16, 20, 30, and 40 V. Naturally, also for these results higher voltage and lower frequency correspond to higher haze. Here, we examine the states that are derived when the chirality of the LC is linked to the LC EHC. As a result of the experiment, the focal conic state (F-state) was generated and maintained for a long time when the voltage was removed at an appropriate frequency to generate DSM2 in the LC cell with the appropriate chiral dopant (Fig. S5(a)), when the electric field was removed from the voltage at which DSM1 was generated, a mixed state (M state) in which the F-state-and P-states

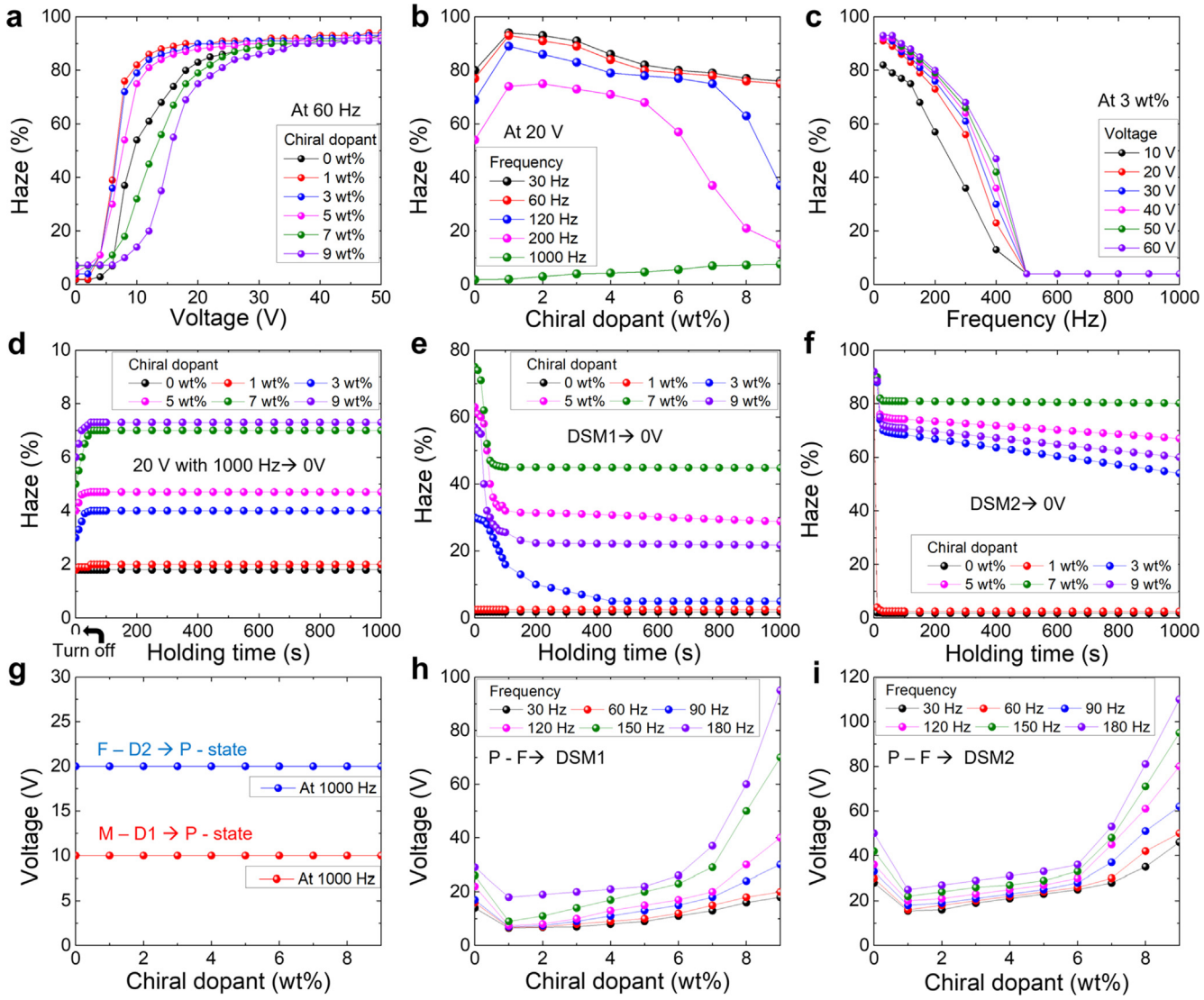

Fig. 3. Haze change for several parameters and holding time of each stable state. (**a**) Haze depending on voltage of 60 Hz at several chiral concentrations. (**b**) Haze depending on chiral concentration at several frequencies of voltage of 20 V. (**c**) Haze depending on frequency at several voltages for chiral concentration of 3 w%. (**d**) Holding time of P-F at turned off voltage after applying 20 V with 1000 Hz at several chiral concentrations. (**e**) Holding time of M−D1 after turned off voltage from DSM1 for several chiral concentrations. (**f**)Holding time of F-D2 after turned off voltage from DSM2 for several chiral concentrations. (**g**) Voltages generating P-state from F-D2 and M−D1 for chiral concentrations at 1000 Hz. (**h**) Voltages generating M−D1 from P-F for chiral concentrations at several frequencies. (**i**) Voltages generating F-D2 from P-F for chiral concentrations at several frequencies.

were mixed was generated (Fig. S5(b)). And the planar state was maintained for a long time, even when the electric field was removed (Fig. S5(c)). This appears to be different from the generation method of typical cholesteric states using a normal positive-dielectric anisotropic LC. For the conventional cholesteric LC, the F-state and P states were generated by adjusting the switching time in which a strong electric field was removed after being applied in the vertical direction. However, it is difficult to obtain a stable P-state without rubbing on the alignment layer, and it was difficult to obtain a stable F-state when rubbing; thus, it was not easy to fabricate a bistable cholesteric LC cell. In this study, when LCs with negative dielectric anisotropy contained a chiral dopant at a concentration of 3 wt% or higher, the LCs were arranged horizontally; thus, even if a vertical electric field was applied, the LCs were not arranged in the vertical direction. Therefore, unlike the existing cholesteric driving principle of generating P-state and F-states by adjusting the switching time to remove the electric field after aligning the LCs with a strong electric field, the generation of P- and F-states appears to be related to the convection flow of the LCs. DSM2, in which LCs move randomly without directionality due to strong turbulence, easily generates randomly twisted F-states; when a convection flow is not generated at a voltage of 1000 Hz or higher, well-aligned P-states are likely to be generated. Therefore, DSM1, with some directionality due to relatively weak turbulence, becomes neutral with respect to P-state and F-states. The three stable states, F-state coupled with DSM2 (F-D2), P-state depending on frequency (P-F), and M−state linked to DSM1 (M−D1) generated by LC EHC, are very stable and have a low switching voltage compared to the conventional cholesteric LC cells. To determine the stability of each stable state generated in the UV-irradiated chiral LC cell, we investigated the retention time of each stable state with respect to the chiral concentration. Fig. 3(d) shows the holding time of the stable P-F as a function of the chiral concentration at 20 V and 1000 Hz. This indicated that the initial state was maintained for a long time at all chiral concentrations. The variation in the haze with chiral concentration was due to the changes in the degree of twisting. However, the 0 and 1 wt% samples were vertically oriented, resulting in a transparent state with very low haze (Figure S6). M−D1 maintained the M−state for a long time after stabilization, although the change time from the initial DSM1 to stable M−D1 varied depending on the chiral concentration. After stabilization, the optimal chiral concentration for retention time was 7 wt%, and the retention time decreased to 9 wt% (Fig. 3(e)). This may also be due to the different

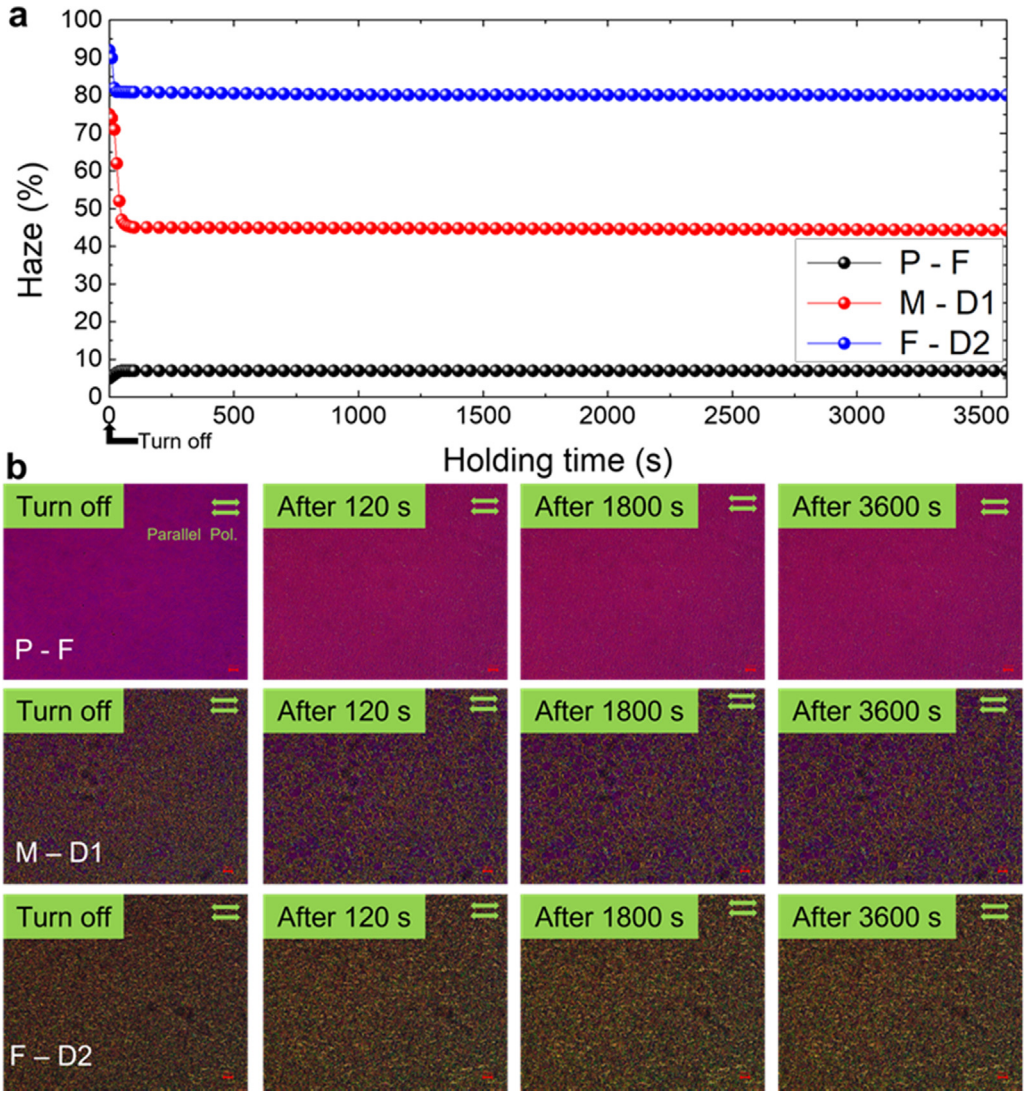

Fig. 4. Tri-stable-hazy state. (**a**) Holding times of haze for P-F, M−D1, and F-D2 at UV irradiated LC cell with chiral concentration of 7 w%. (**b**) Microscopic images showing stability of each stable state.

convection activities depending on the chirality of the LCs. F-D2 was also optimized when the chiral concentration was 7 wt% after state stabilization. At other chiral concentrations, the haze decreased slightly over time; however, at 7 wt%, the haze remained almost constant. Then, the voltage required for switching to P-state under electric field, DSM1, and DSM2 from the stable states for various frequencies depending on the chiral concentration was determined. Fig. 3(g) shows the voltage required to change from F-D2 and stable M−D1 to P-F with a 1000 Hz electric field depending on the chiral concentration. Regardless of the chiral concentration, the switching voltage is constant, and it is also known that the voltage required to transition from the F-D2 state to the P-state with the electric field is higher than the voltage required to transition from the M−D1 to the P-state. As expected, it was observed that with the exception of the 0 wt% sample, the voltages required to transition from the P-F to DSM1 and DSM2 increase with increasing chiral concentration and frequency (Fig. 3(h-i)).

From the viewpoint of the maintenance time of stable states and the switching voltage to DSM2, the optimized chiral dopant amount was 7 wt%, which is in the infrared region with a pitch of 1400 nm. Thus, the P-F becomes highly transparent. Fig. 4(a) shows the retention time of each stable state for the optimized amount of chiral dopant in more detail. F-D2 and P-F were almost permanently maintained (See video). On the other hand, it was found that the mixed state in which the P-F and F-D2 were mixed was maintained for approximately an hour with the haze change within 3 %. Therefore, if the switching voltage to DSM1 is applied once per hour by electrical control, M−D1 can be maintained in a stable state. The amount of power consumed for such an hourly application of electrical control is quite small and is not a burden on power consumption. Fig. 4(b) shows microscopic images indicating that the three states did not change over time.

Fig. 5 shows schematics of the driving voltage to realize the low-power-consumption tri-stable state smart window and diagrams illustrating the various states that appear in the switching. To indicate an appropriate hazy state, regardless of the identity of the previous state, if a 15–20 V switching voltage at 300 Hz or less is applied to the electrode, the DSM1 with a weak haze appears, and if the voltage is turned off, M−D1 that exhibits a translucent state in a smart window is obtained. This translucent state may be preferred by consumers during the day because people inside near the window can see the outside view,+ but the people outside far from the window cannot see the images of the room. To display a higher hazy state, if a voltage of 20 V or greater with a frequency of 300 Hz or less is applied to the electrode, the DSM2 with a deep haze appears, and if the voltage is turned off,

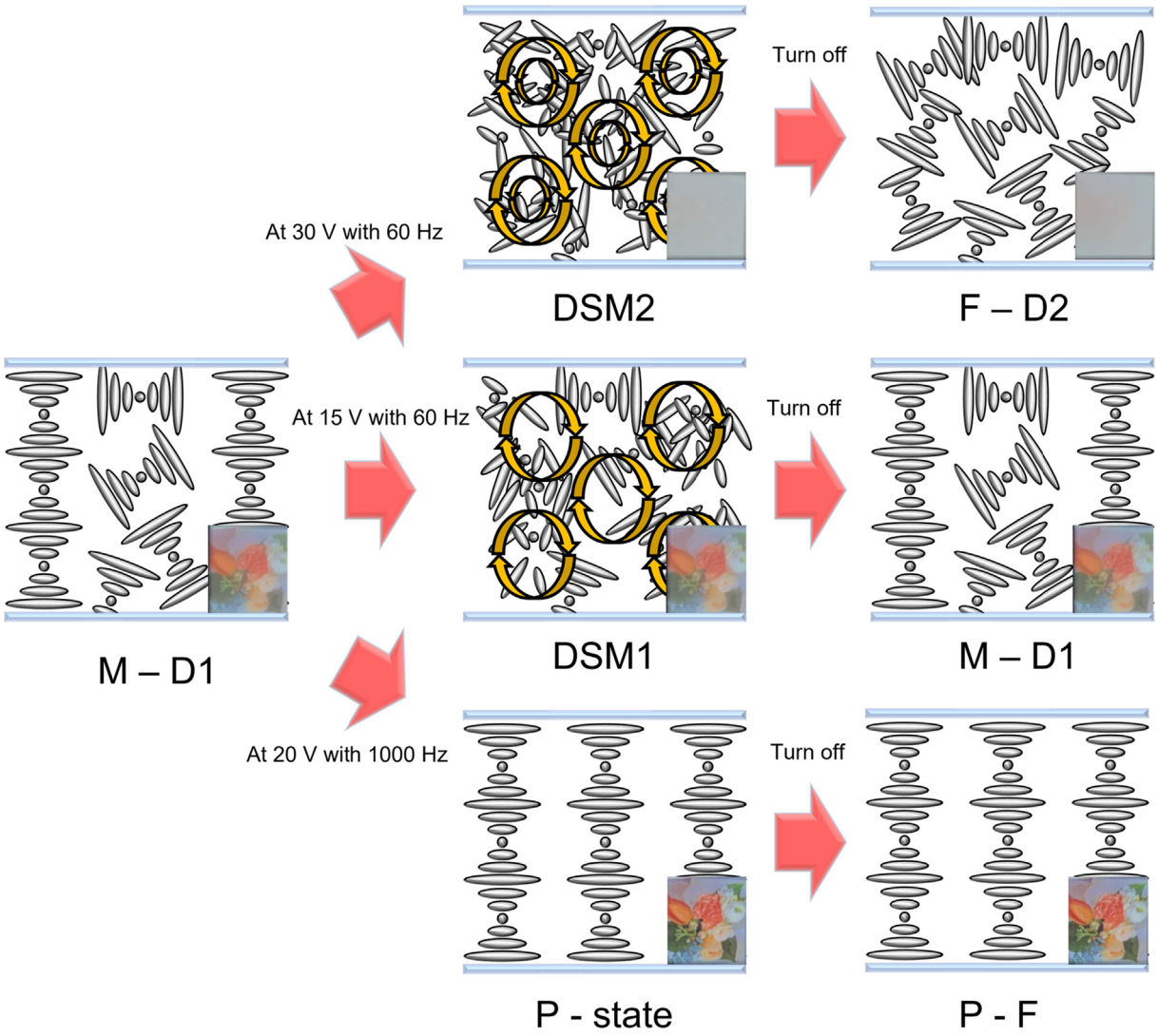

Fig. 5. Driving schematics. A tri-stable state smart window and conceptual diagrams illustrating various states appearing in switching to realize low power consumption.

F-D2 that shows a foggy state in the smart window is obtained. This state may be preferred by consumers at night when the image of the room is easily exposed to the outside.

To obtain the transparent state, if a voltage of 10 V or higher at 1000 Hz or higher is applied to the electrode, the P-F with a highly transparent state appears, and even if the voltage is turned off, it is maintained as a stable state. This state will be preferred when consumers want to see the beautiful scenery outside very clearly.

It is important to obtain stable states of LCs in order to reduce power consumption in the smart window, but it is also important to achieve various haze states to meet the needs of various consumers, even if some power is consumed. Fig. 6 shows that the haze levels can be continuously adjusted through the application of appropriate frequency and voltage in each stable state. Here, it can be seen that the frequency is the main factor determining the variation in the haze when an electric field is applied to the

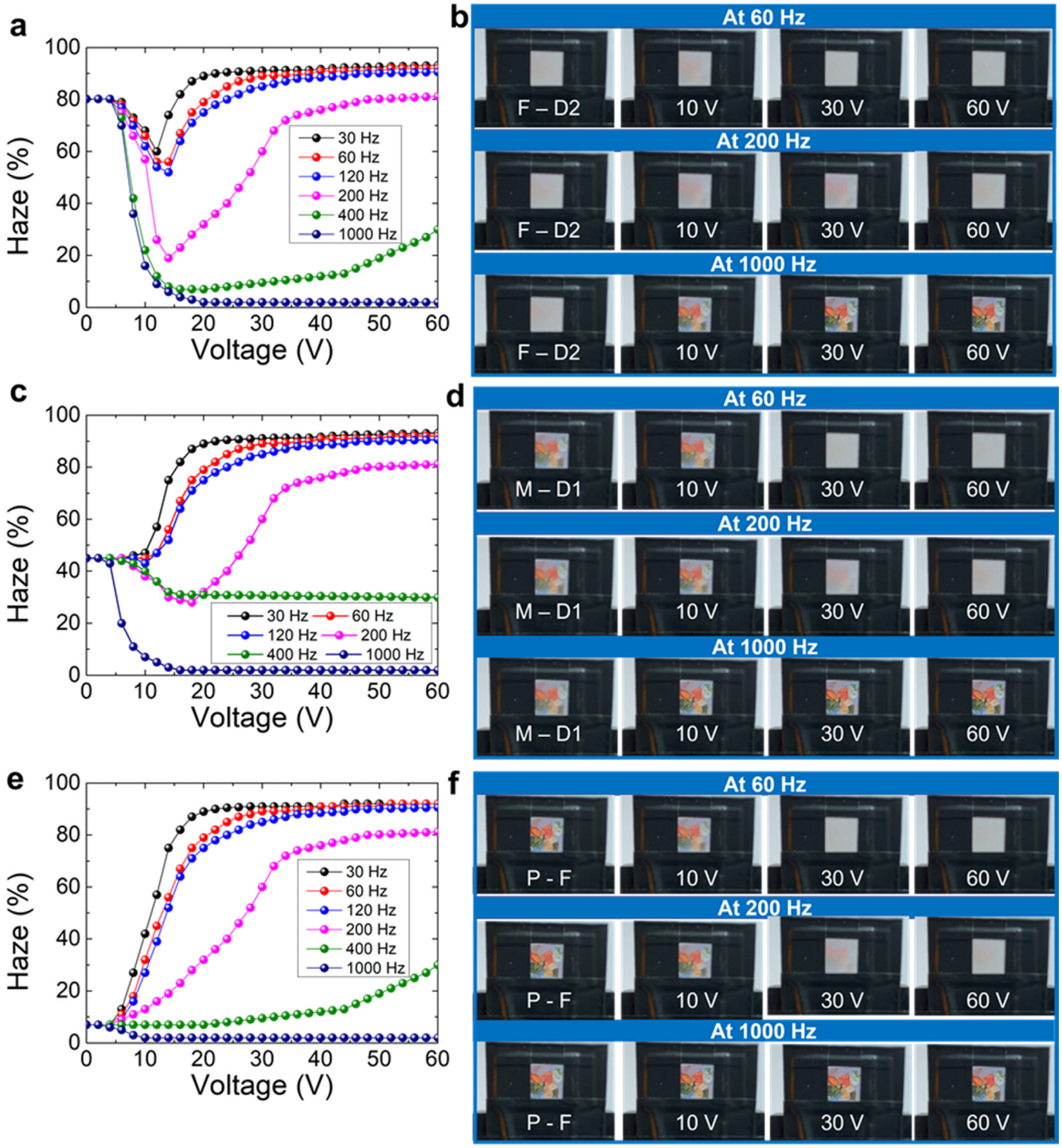

Fig. 6. Haze levels. (**a**) Haze levels through frequency and voltage in initial F-D2. (**b**) Photo images of an LC cell showing results of Fig. 6 **(a). (c)** Haze levels through frequency and voltage in initial M−D1. (**d**) Photo images of an LC cell showing results of Fig. 6 **(c). (e)** Haze levels through frequency and voltage in initial P-F. (**f**) Photo images of an LC cell showing results of Fig. 6**(e)**.

LC cell. In the relatively low-frequency region, when an electric field is applied, the haze increases, and in the relatively high-frequency region, the haze decreases. The haze in the initial stable F-D2 changed with increasing voltage. At 30 and 60 Hz, the haze increased to 93 % with increasing voltage, but at 1000 Hz, it decreased continuously to 3 % (Fig. 6(a)). Eventually, it can be observed that all haze levels can be expressed by frequency variation. The results in Fig. 6(a) can be confirmed through photographs of an LC cell obtained at different voltages at each frequency (Fig. 6 (b)). The haze in the initial stable M−D1 also changed with an increase in the voltage at several frequencies. This shows a tendency similar to that shown in Fig. 6(a) (Fig. 6(c)). The results in Fig. 6(c) can be confirmed through photographs of an LC cell obtained at different voltages at each frequency (Fig. 6(d)). This shows that the p-state is more transparent under a high-frequency electric field than the P-F state. At a low frequency, the haze can be continuously increased from 7 to 92 % by adjusting the voltage.

(Fig. 6(e)). The results in Fig. 6(e) can be confirmed through photographs of an LC cell obtained at different voltages at each frequency (Fig. 6(f)).

In this work, to increase the retention time of each stable state, a change in the switching time may be considered. In fact, if the voltage gradually decreases and is turned off for the transition from the DSM2 to the F-state, another stable state with different haze levels can be obtained (Figure S7). Of course, the transition from the DSM1 to the M−state also showed similar results.

According to the switching time, the composition ratio of the P- and F-states comprising the M−state in the LC cell changes, and various haze events can occur in a stable state. The various driving methods for CNLC cells combined with LC convection should be studied further in the future. For application, in the case of a cholesteric LC with a wider reflective spectrum, smart window with a P-F that reflects infrared radiation from the sun may be useful in the summer. As an additional function of the proposed smart window, in addition to the low switching voltage and low power consumption, the infrared shutter function will be enabled for the next generation of smart window.

4. Conclusion

In conclusion, we presented a smart window technology with low power consumption and low driving voltage based on LC electroconvection. we showed that electrohydrodynamic convection of UV-treated CNLCs generates stable hazy states. To reduce the driving voltage, LCs were irradiated with strong UV to dramatically activate LC electroconvection without any ion additives. UV-irradiation produces relatively heavier and larger molecular ion in CNLCs, which activates electroconvection, and leads to easily dynamic scattering mode (DSM) with strong turbulence without dielectric breakdown. Chirality of LC combined with the DSM builds two stable states (planar state and focal conic state) more strongly, unlike the conventional method generating the two states in the CNLCs. The heavy and large molecular ion effect enables state conversion to a much lower switching voltage than that of the conventional cholesteric devices. The focal conic state connected to DSM2 exhibits a stable deep hazy state, the mixed state combined with DSM1 displays a stable weak hazy state, and the planar state activated in a particular frequency region creates a stable and very clear transparent state due to the chiral pitch of the infrared region. The tri-stable-hazy state can be applied to smart window specialized in low power consumption, excellent viewing angle, low manufacturing cost, and low voltage driving. Therefore, the proposed smart window technology is suitable for commercial use in the next-generation window shutters.

The authors benefited from the discussions with Prof. Dae Won Cho.

CRediT authorship contribution statement

Jeong Won Ryu: Validation, Investigation, Data curation. **Gyu-Jin Choi:** Validation, Investigation, Data curation. **Chao Ping Chen:** Resources, Writing – review & editing. **Chul Gyu Jhun:** Methodology, Formal analysis, Writing – original draft, Writing – review & editing, Supervision. **Jin Seog Gwag:** Conceptualization, Writing – review & editing, Supervision, Funding acquisition.

Data availability

Data will be made available on request.

Declaration of Competing Interest

The authors declare that they have no known competing financial interests or personal relationships that could have appeared to influence the work reported in this paper.

Acknowledgements

This work was supported by the National Research Foundation of Korea (NRF) grant funded by the Korea government (MIST) (No. 2022R1A2C1012996), National Natural Science Foundation of China (61901264, 61831015), Science and Technology Commission of Shanghai Municipality (19ZR1427200).

Appendix A. Supplementary material

Supplementary data to this article can be found online at https://doi.org/10.1016/j.molliq.2022.120467.

References

[1] S. Liu, Y.W. Du, C.Y. Tso, H.H. Lee, R. Cheng, S.P. Feng, K.M. Yu, Organic Hybrid Perovskite (MAPbI3−xClx) for Thermochromic Smart Window with Strong Optical Regulation Ability, Low Transition Temperature, and Narrow Hysteresis Width, Adv. Funct. Mater 31 (2021) 2010426, https://doi.org/10.1002/adfm.202010426.

[2] Y.Q. Feng, M.L. Lv, M. Yang, W.X. Ma, G. Zhang, Y.Z. Yu, Y.Q. Wu, H.B. Li, D.Z. Liu, Y.S. Yang, Application of New Energy Thermochromic Composite Thermosensitive Materials of Smart Windows in Recent Years, Molecules 27 (2022) 1638, https://doi.org/10.3390/molecules27051638.

[3] Y. Tao, X. Fang, H. Zhang, G. Zhang, J. Tu, L. Shi, Impacts of thermo-optical properties on the seasonal operation of thermochromic smart window, Energy Convers. Manage 252 (2022), https://doi.org/10.1016/j.enconman.2021.115058 115058.

[4] S.J. Lee, S.H. Lee, H.W. Kang, S. Nahm, B.H. Kim, H. Kim, S.H. Han, Flexible electrochromic and thermochromic hybrid smart window based on a highly durable ITO/graphene transparent electrode, Chem. Eng. J 416 (2021), https://doi.org/10.1016/j.cej.2021.129028 129028.

[5] J. Wang, L. Zhang, L. Yu, Z. Jiao, H. Xie, X.W. Lou, X.W. Sun, A bi-functional device for self-powered electrochromic window and self-rechargeable transparent battery applications, Nat. Commun. 5 (2014) 4921, https://doi.org/10.1038/ncomms5921.

[6] R. Goei, A.J. Ong, T.J. Hao, L.J. Yi, L.S. Kuang, D. Mandler, S. Magdassi, A.I.Y. Tok, Novel Nd–Mo co-doped SnO2/α-WO3 electrochromic materials (ECs) for enhanced smart window performance, Ceram. Int. 47 (2021) 18433–18442, https://doi.org/10.1016/j.ceramint.2021.03.167.

[7] S. Kumar, D. Kang, V.H. Nguyen, N. Nasir, H. Hong, M. Kim, D.C. Nguyen, Y.-J. Lee, N. Lee, Y. Seo, Application of Titanium-Carbide MXene-Based Transparent Conducting Electrodes in Flexible Smart Windows, ACS Appl. Mater. Interfaces 13 (34) (2021) 40976–40985, https://doi.org/10.1021/acsami.1c12100.

[8] C.S. Lee, T.A. Kumar, J.H. Kim, J.H. Lee, J.S. Gwag, G.D. Lee, S.H. Lee, An electrically switchable visible to infra-red dual frequency cholesteric liquid crystal light shutter, J. Mater. Chem. C 6 (2018) 4243–4249, https://doi.org/10.1039/C8TC00368H.

[9] J. Wang, C. Meng, C.-T. Wang, C.-H. Liu, Y.-H. Chang, C.-C. Li, H.-Y. Tseng, H.-S. Kwok, Y. Zi, A fully self-powered, ultra-stable cholesteric smart window triggered by instantaneous mechanical stimuli, Nano Energy 85 (2021) 105976, https://doi.org/10.1016/j.nanoen.2021.105976.

[10] H. Liu, Z.H. Guo, F. Xu, L. Jia, C. Pan, Z.L. Wang, X. Pu, Triboelectric-optical responsive cholesteric liquid crystals for self-powered smart window, E-paper display and optical switch, Sci. Bull. 66 (19) (2021) 1986–1993, https://doi.org/10.1016/j.scib.2021.05.016.
[11] S.W. Oh, S.M. Ji, C.H. Han, T.H. Yoon, A cholesteric liquid crystal smart window with a low operating voltage, Dyes Pigm. 197 (2022), https://doi.org/10.1016/j.dyepig.2021.109843 109843.
[12] H. Zhang, P. Yu, T. Zhong, Y. Zhao, Z. Miao, Z. He, K. Li, Y. Zhang, Y. Zhao, W. Shen, Preparation of chiral polymer/cholesteric liquid crystals composite films with broadband reflective capability for smart windows and thermal management of buildings, Optic, Mater. 121 (2021), https://doi.org/10.1016/j.optmat.2021.111611 111611.
[13] H. Shin, J.W. Ryu, J.S. Gwag, H.-M. Lee, J.-Y. Hong, S.-W. Kim, Y.-S. Lee, J.M. Kim, Temperature controllable liquid crystal window shutter, J. Korean Phys. Soc. 80 (3) (2022) 273–278, https://doi.org/10.1007/s40042-022-00422-0.
[14] I. Mondal, S. Kiruthika, M.K. Ganesha, M. Baral, A. Kumar, S. Vimala, P.L. Madhuri, G.G. Nair, S.K. Prasad, A.K. Singh, G.U. Kulkarni, ITO-free large area PDLC smart windows: a cost-effective fabrication using spray coated SnO 2 on an invisible Al mesh, J. Mater. Chem. A 9 (2021) 23157–23168, https://doi.org/10.1039/D1TA05820G.
[15] Y. Zhang, J. Chen, X. Hu, W. Zhao, D.J. Broer, G. Zhou, Reverse Mode Polymer Dispersed Liquid Crystal-based Smart Windows: A Progress Report. Rec. Prog. Mate. 3 (2021) 21926. http://dx.doi.org/10.21926/rpm.2104044.
[16] S.T. Tang, H.W. Chiu, M.C. Tseng, H.S. Kwok, 12.2: Narrow Angle Scattering Measurement of PDLC/PNLC Smart Window, International Conference on Display Technology 52 (2021) 78–81, https://doi.org/10.1002/sdtp.14382.
[17] B. Zhou, C. Che, Y. Li, C. Wang, Y. Wu, W. Chang, Y. Xiao, X. Cao, G. Lin, X. Song, Y.i. Zhou, Dielectric reorientation and electrohydrodynamic instabilities in dichroic-dye-doped dual-cell liquid crystal smart window, Liq. Cryst. 49 (1) (2022) 111–122, https://doi.org/10.1080/02678292.2021.1945692.
[18] C. Meng, E. Chen, L. Wang, S. Tang, M. Tseng, J. Guo, Y. Ye, Q.F. Yan, H. Kwok, Color-switchable liquid crystal smart window with multi-layered light guiding structures, Opt. Express 27 (2019) 13098, https://doi.org/10.1364/OE.27.013098.
[19] J. Wang, C. Meng, Q. Gu, M.C. Tseng, S.T. Tang, H.S. Kwok, J. Cheng, Y. Zi, Normally Transparent Tribo-Induced Smart Window, ACS Nano 14 (2020) 3630–3639, https://doi.org/10.1021/acsnano.0c00107.
[20] J.H. Huh, N. Miyagawa, Reentrant prewavy instability in competition between rising and twist modes in ac field-driven electroconvection, Phys. Rev. E 103 (2021), https://doi.org/10.1103/PhysRevE.103.062701 062701.
[21] D.G. Ryu, G.J. Choi, R.K. Mishra, J.S. Gwag, et al., Anchoring energy of nematic liquid crystals on zinc oxide film, J. Korean Phys. Soc. 78 (2021) 307–314, https://doi.org/10.1007/s40042-021-00071-9.
[22] G.J. Choi, J.M. Song, C.G. Jhun, J.H. Huh, J.S. Gwag, et al., Visual evaluation of surface anchoring strength by electrohydrodynamic convection of a nematic liquid crystal, Phys. Rev. E 96 (2017), https://doi.org/10.1103/PhysRevE.96.040701 040701.
[23] D.G. Ryu, J.H. Huh, Y.K. Kim, J.S. Gwag, et al., Characterization of surface anchoring energy of nematic liquid crystals via electrohydrodynamic instability, Phys. Rev. E 101 (2020), https://doi.org/10.1103/PhysRevE.101.062703 062703.
[24] C.G. Jhun, G.J. Choi, D.G. Ryu, J.H. Huh, J.S. Gwag, State transition at electrohydrodynamic convection of twisted nematic liquid crystals, Phys. Rev. E 98 (2018), https://doi.org/10.1103/PhysRevE.98.052704 052704.
[25] M. Shiomi, E.J. Choi, J.H. Huh, Prewavy instability-originated dielectric chevrons of electroconvection in nematic liquid crystals, Phys. Rev. E 102 (2020), https://doi.org/10.1103/PhysRevE.102.042704 042704.
[26] J.W. Huh, S.W. Oh, J.H. Seo, H.J. Sohn, T.H. Yoon, Filtering of yellow light in a liquid-crystal light shutter for higher color contrast and reduced glare, J. Mol. Liq. 327 (2021), https://doi.org/10.1016/j.molliq.2020.114846 114846.
[27] S. Cai, Z. Wang, L. Lu, T.A. Zaki, G.E. Karniadakis, DeepM&Mnet: Inferring the electroconvection multiphysics fields based on operator approximation by neural networks, J. Comput. Phys. 436 (2021), https://doi.org/10.1016/j.jcp.2021.110296 110296.
[28] S. Felix, M. Schatz, M. Habermann, J. Linkhorst, A. Mani, M. Wessling, Direct 3D observation and unraveling of electroconvection phenomena during concentration polarization at ion-exchange membranes, J. Membr. Sci. 640 (2021), https://doi.org/10.1016/j.memsci.2021.119846 119846.
[29] V.V. Gil, M.V. Porozhnyy, O.A. Rybalkina, K.G. Sabbatovskiy, V.V. Nikonenko, Modification of a heterogeneous cation-exchange membrane by Ti-Si based particles to enhance electroconvection and mitigate scaling during electrodialysis, Electrochim. Acta 391 (2021), https://doi.org/10.1016/j.electacta.2021.138913 138913.
[30] Y. Zhang, X. Yang, Y. Zhan, Y. Zhang, J. He, P. Lv, D. Yuan, X. Hu, D. Liu, D.J. Broer, G. Zhou, W. Zhao, et al., Electroconvection in Zwitterion-Doped Nematic Liquid Crystals and Application as Smart Windows, Adv. Opt. Mater 9 (2021) 2001465, https://doi.org/10.1002/adom.202001465.
[31] W. Helfrich, Molecular Theory of Flow Alignment of Nematic Liquid Crystals, J. Chem. Phys. 50 (1) (1969) 100–106, https://doi.org/10.1063/1.1670765.
[32] R. Dabrowski, J. Dziaduszek, J. Bozetka, W. Piecek, R. Mazur, M. Chrunik, P. Perkowski, M. Mrukiewicz, M. Żurowska, D. Weglowska, Fluorinated smectics - New liquid crystalline medium for smart windows and memory displays, J. Mol. Liq. 267 (2018) 415–427, https://doi.org/10.1016/j.molliq.2017.12.068.